Acoustic Detection of Cracks and Delamination in Multilayer Ceramic Capacitors

Saku Levikari ⓘ *, Member, IEEE*, Tommi J. Kärkkäinen ⓘ *, Member, IEEE*, Caroline Andersson ⓘ *, Member, IEEE*, Juha Tammminen, and Pertti Silventoinen, *Member, IEEE*

Abstract—Multilayer ceramic capacitors (MLCC) are the most widely used capacitor type in the electronics industry. However, the brittle ceramic dielectric makes MLCCs prone to mechanical damage. Manufacturing defects or damage during board assembly may cause a capacitor to prematurely fail during its operational life. Here, we demonstrate the fast and non-destructive acoustic screening of MLCCs. Soldered 2220-sized MLCCs were subjected to ac voltage frequency sweeps, causing them to vibrate mechanically. Acoustic responses of the capacitors were measured before and after subjecting the test circuit board to severe bending. The results show that the cracks and delaminations caused by bending induce characteristic changes in the capacitors' acoustic response. A support vector machine classifier was trained to successfully detect damaged capacitors based on their acoustic response.

Index Terms—Acoustic emission, ceramic capacitors, nondestructive testing.

I. INTRODUCTION

MULTILAYER ceramic capacitors (MLCCs) are commonly used in the electronics industry [1]. The ceramic dielectric gives MLCCs high capacitance per volume, but also makes them prone to mechanical damage.

Voids and delaminations are typical manufacturing defects in MLCCs, often related to thermal stresses [2], [3]. Mechanical stress, such as improper printed circuit board (PCB) handling during assembly, can lead to cracks or delamination in MLCCs [4], [5]. Mechanical damage in MLCCs is often left unrecognized during production or assembly, as the capacitor may operate normally electrically. However, in the field, a crack or delamination in an MLCC may grow in size, resulting in loss of

capacitance, shortened lifespan, or an open or short contact [6]. Larger case size capacitors, used in, e.g., power electronics, have shown to be more prone to damage from PCB bending than the more commonly used cases in the 0402 to 1206 range [7]. Testing the capacitors at the assembly line of the system would prevent unexpected damage in the field. At this moment, however, a suitable quality assurance, or production testing method does not exist.

Defects or damage in MLCCs can be detected by mechanical microsectioning [8] and chemical etching [9], but these methods are destructive for the capacitor and are therefore unsuitable for production testing. Recently, an X-ray imaging method with sufficient accuracy for reliable crack detection has been proposed [10]. Delamination defects, however, cannot be seen in X-ray images. Other proposed nondestructive methods include ultrasound imaging [5], acoustic emission counting using a mechanical ram [6], impedance analysis under dc bias [11], leakage current monitoring [12], laser speckle pattern analysis [13], opto-acoustic microscopy [14], and neutron radiography [15].

In this paper, the quality assurance testing goal is approached by measuring the acoustic phenomena of the MLCCs. When under ac voltage, MLCCs generate acoustic emissions. Acoustic emissions are physical vibrations caused by the piezoelectric properties of the dielectric ($BaTiO_3$) [16], [17]. Recently, it was shown that a narrow-pulse frequency sweep signal can be used to produce vibration in MLCCs, and that bending the circuit board in order to produce cracks in the MLCCs changes the acoustic emission characteristics of the capacitors [18]. Similar findings have been made by Johnson *et al.* using resonant ultrasound spectroscopy [19]–[21]. The acoustic approach is particularly interesting, since there is a need in the industry for a method that could identify damaged capacitors from an assembled board. Acoustic monitoring has also been applied for other electronic components, such as power semiconductor modules [22]–[24].

The term *acoustic emission* does not necessarily refer to audible sounds in the human hearing range. Indeed in this context, the authors use the term as a synonym for vibration occurring in the capacitor, caused by the electromechanical phenomena within the capacitor itself.

In this study, acoustic signals produced using the method from [18] are measured using a point contact sensor. Acoustic measurements are conducted before and after bending the circuit board. The measured waveforms are then analyzed and correlated against bending-induced damage in the capacitors. In order to determine the suitability of acoustic measurements for

Type	Pulse wave
Duration	100 ms
Frequency range	100 Hz . . . 2 MHz
Voltage	−10 V . . . + 10 V
Duty cycle	80%
Frequency slope	linear

detection of physical damage, a support vector machine (SVM) [25] is trained on the acoustic data to classify the MLCCs as either damaged or undamaged. The key observation from the data is that the changes in the acoustic emission correlate quite well to delamination of the end termination in the capacitors, better than to the existence of cracks. This suggests that it may be possible to develop a delamination detection method based on acoustic emission. Such a method would be very welcome, because at the moment a non-destructive test method for finding delamination in MLCCs does not exist. The acoustic measurement may be useful in identifying cracked capacitors as well, even though the correlation in the analyzed signals is not as good as it is for delamination.

This paper has been improved from its original form, published in the SDEMPED 2017 conference [26].

II. EXPERIMENT

The experiment was conducted on 60 2220-sized MLCC capacitors of 22 μF, assembled on a purpose-built PCB. Half of the capacitors were flexible end termination capacitors, while the others had "normal" end terminations.

The experimental procedure was as follows: first, the capacitors were characterized individually by driving them with frequency-swept voltage while measuring their acoustic emissions using a point contact sensor. The test board was then subjected to a controlled bending to damage the MLCCs. After bending, the capacitors were re-characterized acoustically. X-ray imaging and cross-sectioning were used to obtain accurate information on the actual condition of each capacitor.

After obtaining all the data described above, changes observed in the acoustic data were compared to the damage observed in each capacitor. In addition to 2220-sized MLCCs, the effect of circuit board bending has also been acoustically observed in case of sizes 1206, 1210, and 1812, all of which yield stronger acoustic response than 2220 [27]. Because PCB bending-caused flex cracks have been an issue especially with larger case sizes, this study was performed on 2220-size capacitors. The acoustic data, alongside X-ray and cross-sectioning results, are publicly available [28].

A. Acoustic Characterization

To obtain an acoustic response, the MLCCs were driven with a pulse frequency sweep signal specified in Table I. A KRN Services KRNBB-PC broadband point contact sensor was attached to the capacitor being characterized (see Fig. 1). The signal was amplified using a KRN AMP-1BB-J measurement amplifier and then recorded using a Keysight MSO-X 4104A
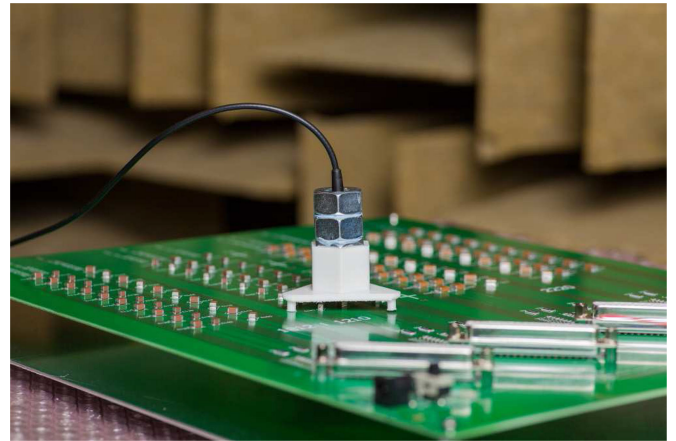

Fig. 1. Point contact sensor placed on top of a capacitor. The sensor is within a 3-D printed fixture on the test PCB, allowing the sensor to be in place without holding it manually.

oscilloscope. The test was conducted in an anechoic room in order to minimize any external acoustic disturbances.

The signal from the point contact sensor contains a significant amount of electromagnetic interference (EMI). The harmonics of the pulsed input signal also excite the resonant frequencies of an MLCC to appear several times during a sweep [18]. Moreover, at frequencies below 50 kHz, a high-amplitude burst likely related to PCB vibration occurred in most of the measurements.

To remove the harmonics and EMI, the signals were processed using wavelet decomposition and low-pass filtering. After these stages, the envelope curve of the signal was calculated. The envelope curve is treated as the acoustic response of the capacitor because it is more convenient to compare envelopes than raw acoustic responses.

The acoustic characterization process was conducted in an identical manner before and after bending.

B. Inflicting Damage to the Capacitors

The test board was bent with a Zwick-Roell Z010 four-point bending setup. Under 18-mm bending displacement, the PCB was subjected to strain levels between 5800 and 8000 μStr measured at the board centerline, with an average of 6000 μStr.

In reality, a PCB does not experience uniform bending in one direction, especially directly aligned with the orientation of the capacitor. To take this into account, capacitors were assembled in three different angles relative to the direction of the bending. This affects the type and location of damage within the capacitor.

C. X-Ray Imaging and Cross-Sectioning

After the test board bending, the capacitors were inspected for cracks by X-ray imaging using a Phoenix Nanomex machine. The capacitors were also cross-sectioned to reveal any delamination, which cannot be seen by X-ray. This was done by casting the MLCCs in two-phase epoxy, grinding them with a Struers Rotopol-11 to a desired depth, and then polishing the surface for inspection with a Leica M205C optical microscope.

Cross-sectioning gives accurate information of the condition in the depth that the capacitor has been ground to. If a crack or delamination can be seen in this depth, the capacitor is classified as being damaged. If no damage is seen, however, the existence of damage cannot be ruled out, since a crack or delamination can reside deeper in the capacitor. For this reason, capacitors that showed no damage but exhibited slight changes in their acoustic characteristics were imaged at three different depths to get better understanding of the condition.

The authors would like to point out that cross-sectioning is a very labor-intensive process. It is not feasible to do a complete cross-sectioning of every capacitor at multiple depths. For this reason, full-depth cross-sectioning was not performed for every capacitor.

D. SVM Classification

Intuitive discrimination between damaged and undamaged capacitors by inspecting the acoustic responses is difficult and infeasible. Instead, the classification must be based directly on features of the acoustic data. Because each capacitor will yield different numeric features, reliable classification based on strict conditional expressions would be impracticable. Therefore, the machine learning approach is more suitable for the classification task. SVM are machine learning based binary classifiers that have been successfully utilized in signal classification tasks [25], [29], [30]. In the basic SVM approach, the data consist of samples (in this case, the MLCCs) belonging in either positive (1) or negative (0) category. From each sample, n numerical features are extracted. The samples are then mapped onto an n-dimensional feature space, where each dimension corresponds to a certain feature. The SVM classifier is then trained by fitting a *decision plane* into the sample points such that it separates the points in the positive and negative categories by the largest possible margin. Often in real-world scenarios, the data are not linearly separable, i.e., points in different categories overlap. In such a situation, the data points may be mapped into a transformed feature space using a nonlinear kernel function. Furthermore, a cost function is often employed: data points on the wrong side of the decision surface correspond to a total cost, which is minimized as a part of the decision plane fitting [25].

For the task of classifying capacitors, the SVM was trained by extracting only two features from the raw data. This approach kept the classifier model simple and helped in preventing overfitting. Additionally, two-dimensional feature data were convenient to visualize and use in conjunction with the statistical analysis and visual inspection of acoustic responses.

III. RESULTS

All the acoustic emission envelopes contained a strong resonance peak at circa 500 kHz, related to the fundamental resonance modes of the capacitor body. The authors refer to this peak as the *main peak* of the capacitor. As can be seen in Fig. 2, the value of this peak is almost doubled between the measurements for a capacitor with no damage. This change seems very significant at first, but further results suggest that the doubled value is still not very large. The increase in the peak value

may be explained by better sensor-to-capacitor contact during the second measurement. Another probable explanation is that the 6000 μStr bending actually caused some degree of physical changes that were missed during the X-ray inspection and microsectioning, since cracks and delaminations can be difficult to detect from the images. Some changes can be seen at frequencies lower than that of the main peak, but they are not as significant.

In a capacitor which showed significant delamination in the cross-sectioning (see Fig. 3), the changes are much more pronounced. The main peak value is increased to over four times that of a typical value for a pre-bending measurement. Even though not all delaminated capacitors exhibited values this high, notably increased main peak values were observed in the majority of them. On the other hand, most of the capacitors did not show delamination as significant as in Fig. 3(b), where a clear gap can be seen extending horizontally across the end termination.

At lower frequencies, the changes are comparable to those of an undamaged capacitor. New resonance peaks appear at frequencies higher than that of the main peak, but compared to the main peak, their value is very low.

The main peak of a capacitor with cracks (see Fig. 4) exhibits changes even smaller than the intact capacitor. The cracked capacitor does, however, exhibit a new resonance peak at ca. 800 kHz. The emergence of such a peak was observed in multiple cracked capacitors. The frequency of this peak varies from capacitor to capacitor, and is likely to be affected by the size and location of the crack. Nevertheless, the overall emergence of this peak, referred to as the *secondary peak*, was observed to correlate with the presence of damage. The crack shown in Fig. 4(b) is approximately 500 μm in length and 5 mm in width, extending across the capacitor end termination. Since this crack causes noticeable changes in the capacitors acoustic response [see Fig. 4(a)], it is very likely that also smaller cracks and delaminations cause acoustically observable changes.

To study these peaks and the related damage statistically, the main and secondary peak values were obtained programmatically for every acoustic measurement. For this purpose, the main peak value was defined as the highest peak value at frequencies lower than 700 kHz. The secondary peak value, respectively, was defined as the highest peak value at frequencies higher than 700 kHz. The cross section and X-ray images of every capacitor were examined, and each capacitor was deemed to either have or not have a crack, and to either have or not have delamination.

These results were then used to determine which peak indicates which type of damage (see Fig. 5). It is evident that the higher the main peak value, the more likely a capacitor is to have delamination damage. The secondary peak value, on the other hand, does not exhibit such a direct relation to the emergence of delamination.

The main peak value seems to be a poor tool for identifying cracked capacitors. Fig. 5 does not suggest a clear trend between the main peak value and the likelihood of a crack. On the other hand, a weak trend can be observed between the secondary peak value and the emergence of cracks. However, high secondary peak values are not unambiguously an indication of cracks.
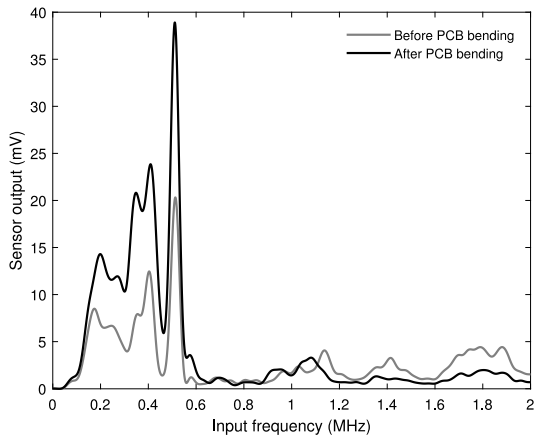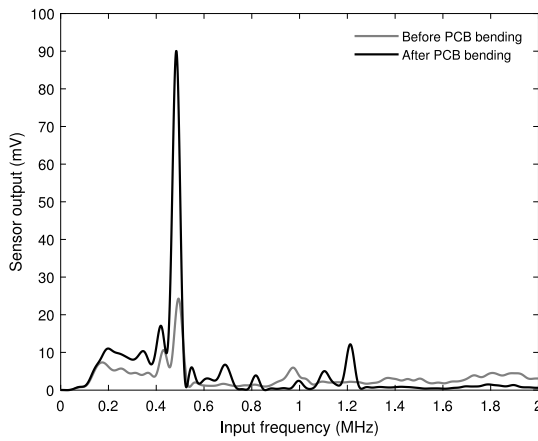
(a) Acoustic response of C198 before and after bending
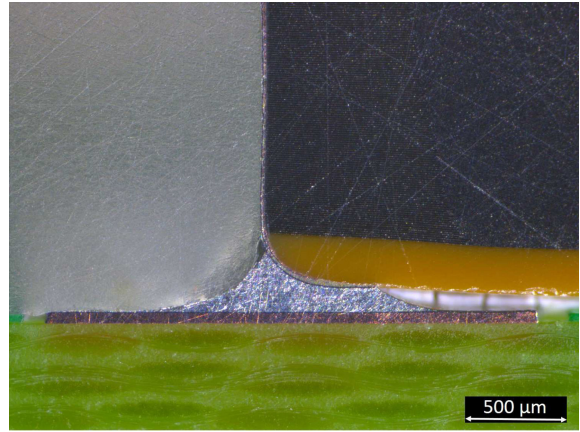
(b) Cross-section of C198 after bending. No cracks or delamination can be seen.

Fig. 2.   Typical example of an MLCC with no observed damage after the bending of the PCB. Slight main peak amplitude increase is seen in (a) at around 500 kHz, but no new resonant peaks are introduced.

(a) Acoustic response of C224 before and after bending
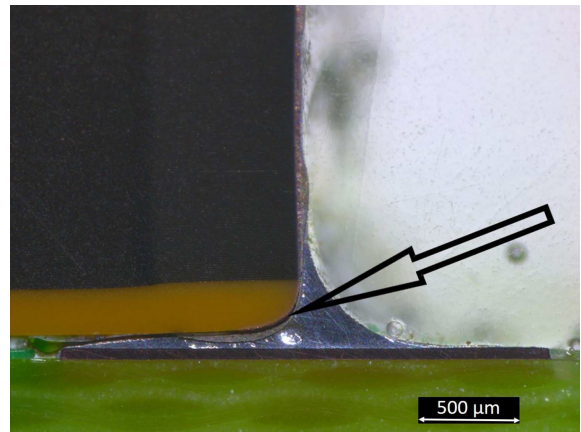
(b) Cross-section of C224 after bending, showing delamination under the right-hand–side termination.

Fig. 3.   Typical example of a capacitor with delamination. The acoustic response in (a) shows significant increase in the main peak value, and several new peaks at different frequencies are introduced above 0.6 MHz.
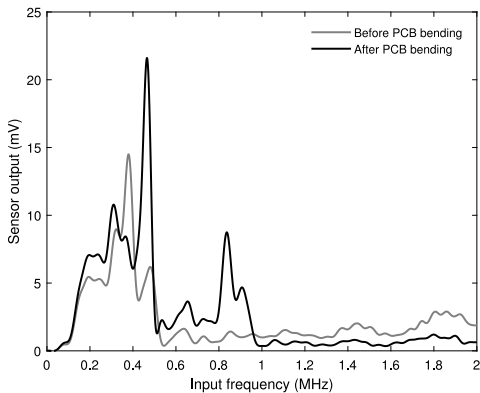
(a) Acoustic response of C201 before and after bending
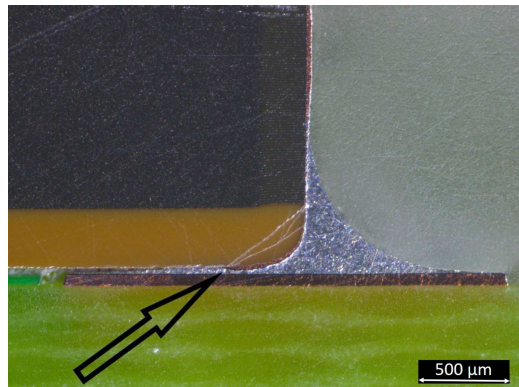
(b) Cross-section of C201 after bending, showing cracks in the passive area near the right-hand–side termination.

Fig. 4.   Typical example of an MLCC with multiple cracks near the termination. Main peak amplitude increase and new resonant peaks around 800 kHz are seen in (a).
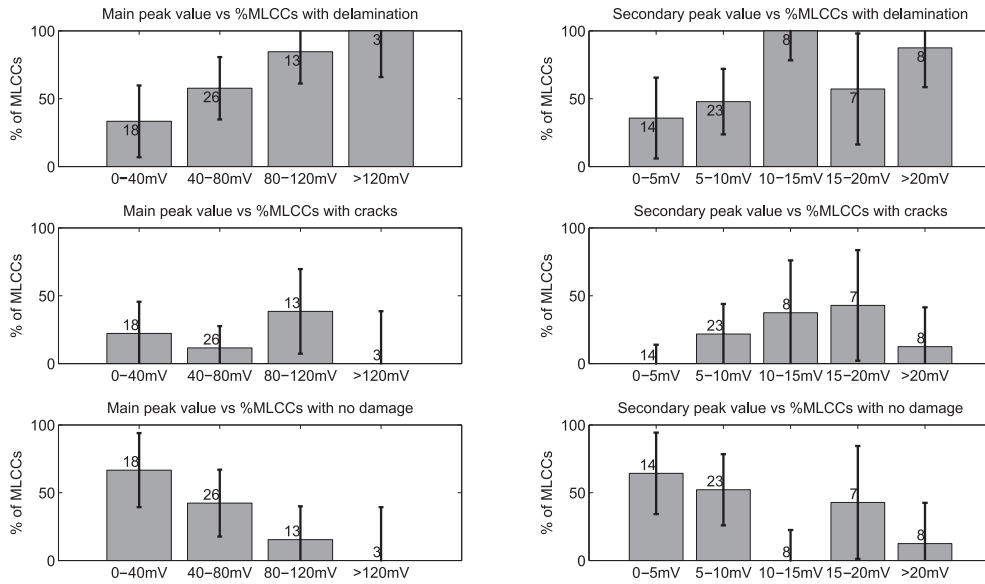
Fig. 5. Histograms describing the relationships amongst cracks, delamination, and acoustic emission peak values of 60 MLCCs. The bins are based on the peak values, and the numbers indicate the total amount of MLCCs in each bin. The error bars depict the combined uncertainty of measurement and sampling errors (see Appendix). Significant correlation between delamination and increased main peak value can be seen, whereas secondary peak values weakly correlate with the occurrence of cracks. Both peak values are generally lower for undamaged capacitors.

Undamaged MLCCs appear to exhibit lower values than damaged capacitors, both in terms of main and secondary peaks. This suggests that an increase in either of the peak values is a possible sign of damage.

A. Detecting Damaged Capacitors Using SVM Classifiers

In order to discriminate between damaged and undamaged MLCCs, an SVM classifier was trained on data extracted from the acoustic measurements. Each MLCC was mapped onto a two-dimensional feature space, with the features being the main and secondary peak values after the PCB bending. Each MLCC was labeled either damaged or undamaged, depending whether or not cracks and/or delamination were observed in the cross-sectioning. The SVM classifier was then trained by fitting a decision surface into the data set as shown in Fig. 6. A Gaussian kernel function was chosen for the SVM model, since it performed better than polynomial kernels. A linear SVM was unable to separate the datapoints properly, whereas using polynomial kernel functions caused the SVM model to overfit into the data.

Because the data set consisted of only 60 MLCCs, dividing it into separate training and validation sets would have had significant negative effect on the performance of the classifier. Instead, *leave-one-out cross validation* [31] was used to evaluate the performance of the classifier: the SVM was trained on data from all but one MLCC, and the performance of the classifier was tested with the left-out MLCC. This procedure was repeated for all 60 MLCCs, simulating the performance of the SVM on data outside the training set.

In classifying undamaged capacitors, the SVM model performed equally well for both in-sample (training) and cross-validated data [see Fig. 7(a) and (b)]. In cross valida-
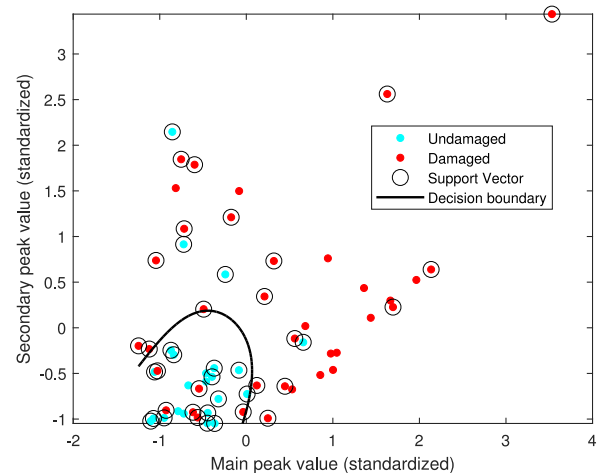

Fig. 6. SVM classifier fitted into observed MLCC features. The peak height data were obtained from the acoustic measurements after bending the PCB. In order to improve the classifier performance, the data were standardized to zero mean and unit variance. Capacitors which showed either delamination and/or cracks in the cross-sectioning are labeled as damaged.

tion, damaged MLCCs were missed by the classifier slightly more often, while the SVM was still able to detect three out of four damaged capacitors. The overall cross-validated accuracy of the classifier was 78.3%, whereas the recall (how many of the damaged capacitors were found) was 75.7%.

The operation of the classifier at different threshold values is visualized by the receiver operating characteristic (ROC) [32] curve in Fig. 8. With out-of-sample data, the SVM classifier performs similarly as with data within the training set. The area under ROC curve (AUROC) with out-of-sample data is approximately 0.78, indicating a fairly good classifier despite the small amount of training data. A perfect classifier would

(a) Confusiuon matrix calculated with values within the training (in-sample) data

(b) Out-of-sample confusion matrix. The values are obtained by pooling the output from each leave-out-one cross-validated model.
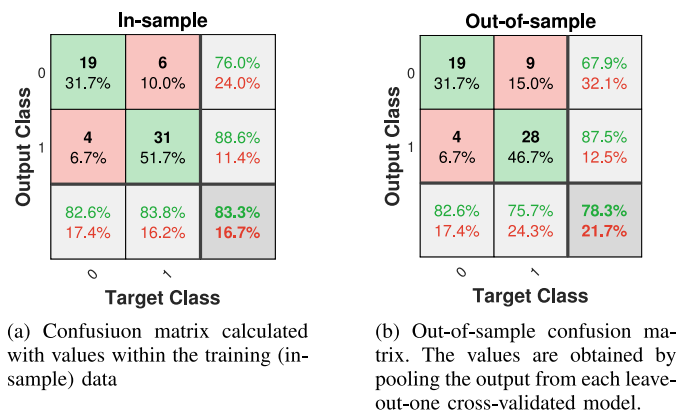
Fig. 7.   SVM classifier confusion matrices for MLCCs in the training data set and combined cross-validation results.
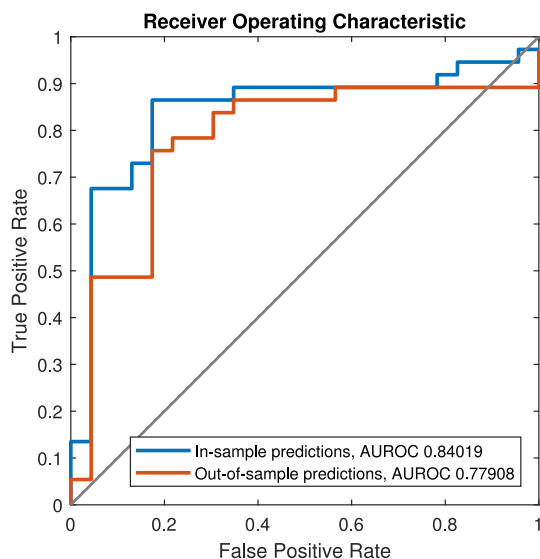

Fig. 8.   ROC of the trained SVM classifier at different output threshold values. AUROC measures the overall performance of the classifier: a perfect classifier has an AUROC of 1.0, whereas pure guessing produces an AUROC of 0.5.

have an AUROC value of 1.0, whereas purely random guessing would produce an AUROC of 0.5. The performance of the classifier could be improved by including more of the features in the acoustic response, provided that the features actually carry information about the condition of a capacitor.

The classification results presented here are for an SVM trained to detect whether or not the capacitor had suffered any kind of damage. Classifiers were also trained to detect specifically either delamination or cracks. Delamination was detected with only slightly lower performance than the combined classifier. For cracks, however, the classifier output was negative for every single capacitor. Unlike in Fig. 6, the cracked capacitors mapped onto the feature space formed no clear cluster for the decision plane to separate from the rest of the data. This suggests that while the main and secondary peak values are enough to determine whether or not an MLCC is delaminated, other features should be extracted if cracks were to be detected.

IV. DISCUSSION

The data obtained in this study suggest that main peak value may turn out to be a valuable metric in identifying delaminated capacitors, especially when used together with secondary peak value information. However, neither of these peak values seem to explicitly indicate the presence of cracks.

In the analysis presented in this paper, only two peak values are taken into account. As it is mentioned in Section III, the secondary peak frequency is not fixed, and varies from capacitor to capacitor. Considering how simple the extracted features are and how small a portion of the frequency response is used, the SVM classifier performs remarkably well. However, capacitors containing only cracks were left undetected.

The determination of delamination and cracks presented in Figs. 5 and 6 is not guaranteed to be error free. The data were obtained by looking at cross section images of the capacitors, and in such a process misidentification is a possibility. Training the SVM model with misidentified capacitors would decrease its accuracy. Nevertheless, the performance of the SVM classifier surpassed the initial expectations of the authors based on visual and statistical observations.

It is likely that by extracting proper features, such as more resonant peaks and their frequency information, the classifier performance would improve both for crack and delamination detection. More flexible classifiers, such as neural networks or random forests could also yield better results; this is a matter for further study. Moreover, the acoustic approach could be used as a complementary method to X-ray analysis, which can identify cracks accurately, but not delaminations.

The cracks and delaminations in this study were relatively small, the vast majority of them residing in the passive region of the capacitors. Nevertheless, even a small fault in a capacitor can grow over time, and water can get inside the component with harmful results. Even though the dimensions of a damaged region cannot be accurately defined by cross section images, damage at the capacitor termination less than 500 μm long can cause changes in the acoustic signature.

Remarkably, the results were identical for flex and "normal" termination capacitors. The authors expected that some difference would be seen between these capacitor types, but this turned out not to be the case. From the production testing point of view, this is a welcome result, as the test method would not have to be redesigned for different termination types.

Even though the capacitors used in this study are physically larger than those found in, e.g., consumer electronics, acoustic screening is applicable for case sizes of 1206 and below [27]. It must also be noted that smaller capacitors are not as prone to damage from bending [7]. Therefore, the most potential applications of acoustic screening are in, e.g., power electronics, where large case sizes and heavy circuit board assemblies increase the risk of flex cracks and delamination.

The physical phenomena causing the changes in the acoustic response has not been discussed yet. It seems likely that delamination near the end terminations of an MLCC allows the capacitor to vibrate more freely in a direction perpendicular to the PCB surface. Because vibration in this direction creates the

largest displacement for the point contact sensor, increase in main peak values is observed. Resonance peaks observed in the secondary peak region have lower amplitude, and thus are likely related to other resonance modes of the capacitor body. A possible explanation for this is that cracks in the ceramic body allow the MLCC to vibrate more freely along these modes, causing secondary peaks to appear.

V. Conclusion

A set of MLCCs was investigated acoustically before and after inflicting damage. The changes in the acoustic characteristics were analyzed and compared against the damage observed in each capacitor. The acoustic data were also used to train an SVM classifier to detect damaged capacitors.

The main finding was that delamination of the capacitor causes quite consistent changes in the acoustic response of a capacitor. Cracks in the capacitor cause changes as well, but are not as easy to detect as those caused by delamination.

The SVM classifier showed promising performance. Nevertheless, further study on feature extraction and classifier algorithms is required to develop a reliable capacitor screening method based on acoustic emission.

Appendix

In order to calculate the error bars for Fig. 5, two major sources of measurement uncertainty were identified: 1) the misidentification of cracks and delaminations in the cross section images, and 2) the sampling error caused by the relatively low number of capacitors in many of the bins in Fig. 5.

Other sources of uncertainty, such as the uncertainty present in the measurement instruments, do exist in this case. It was estimated that their contribution to the total uncertainty of the measurement was insignificant when compared to the uncertainty of the identification of damage and the sampling error.

For the identification of cracks, it was estimated that the likelihood of a false positive, i.e., an intact capacitor being incorrectly determined as having a crack, was 1%. The likelihood of a false negative, i.e., a cracked capacitor being incorrectly determined as being intact, was estimated to be 5%. Similarly, for the identification of delamination, the false positive rate was estimated as 5%, and the true positive rate as 10%.

Using these false identification rates, the maximum and minimum bounds of the error a_+ and a_- were calculated. This yields an asymmetrical distribution of error, which is difficult to handle in the uncertainty estimation process. For this reason, these bounds were converted into a single standard uncertainty value u_1 based on [33, Sec. 4.3.8] as

$$u_1^2 = \frac{a_+ - a_-}{12}. \tag{1}$$

To estimate the effect of sampling error, upper and lower bounds were taken from the chart in [34, p. 494]. In this case, the distribution is heavily skewed, especially in the bins where the number of capacitors is low. The obtained upper and lower bounds were again used to obtain a single standard uncertainty value

$$u_2^2 = \frac{a_+ - a_-}{12}. \tag{2}$$

The two standard uncertainty values were then merged into a combined uncertainty

$$u_c = \sqrt{u_1^2 + u_2^2} \tag{3}$$

which was then multiplied with a coverage factor $k = 1.960$ to expand the uncertainty to a confidence level of 95%. The bar height in Fig. 5 is the observed percentage of capacitors p in each bin, and the error bars cover the range $p \pm ku_c$. The error bars are cut at 100% and 0% because values outside these values are not meaningful.

The authors would like to note that this analysis is heavily simplified. The resulting uncertainty estimates are taken to be good enough for an understanding of how well the results can be generalized to another, similar capacitor population.

References

[1] B.-H. Ko, S.-G. Jeong, Y.-G. Ahn, K.-S. Park, N.-C. Park, and Y.-P. Park, "Analysis of the correlation between acoustic noise and vibration generated by a multi-layer ceramic capacitor," *Microsyst. Technol.*, vol. 20, nos. 8/9, pp. 1671–1677, 2014.

[2] C.-W. Huang, B.-T. Chen, K.-Y. Chen, C.-H. Hsueh, W.-C. Wei, and C.-T. Lee, "Finite element analysis and design of thermal-mechanical stresses in multilayer ceramic capacitors," *Int. J. Appl. Ceramic Technol.*, vol. 12, no. 2, pp. 451–460, Mar. 2015. [Online]. Available: http://search.proquest.com/docview/1660318462?accountid=136582.

[3] T. Adams, "Preventing MLCC failures," *Circuits Assembly*, pp. 17–19, Aug. 20, 2009. [Online]. Available: https://www.circuitsassembly.com/ca/editorial/menu-features/296-current-articles/17452-preventing-mlcc-failures.html

[4] J. A. Ahmar and S. Wiese, "A finite element modelling and fracture mechanical approach of multilayer ceramic capacitors," in *Proc. 16th Int. Conf. Thermal, Mech. Multi-Physics Simul. Experiments Microelectronics Microsystems*, Apr. 2015, pp. 1–5.

[5] T. Adams, "High acoustic frequency imaging," *Ceramic Ind.*, vol. 164, no. 2, pp. 14–16, 2014. [Online]. Available: http://search.ebscohost.com/login.aspx?direct=true&db=bth&AN=94147595&site=ehost-live

[6] S. R. Kahn and R. W. Checkaneck, "Acoustic emission testing of multilayer ceramic capacitors," *IEEE Trans. Compon., Hybrids, Manuf. Technol.*, vol. CHMT-6, no. 4, pp. 517–526, Dec. 1983.

[7] M. Keimasi, M. H. Azarian, and M. G. Pecht, "Flex cracking of multilayer ceramic capacitors assembled with pb-free and tinlead solders," *IEEE Trans. Dev. Mater. Rel.*, vol. 8, no. 1, pp. 182–192, Mar. 2008.

[8] J. M. J. den Toonder, C. W. Rademaker, and C.-L. Hu, "Residual stresses in multilayer ceramic capacitors: Measurement and computation," *J. Elect. Packag.*, vol. 125, no. 4, pp. 506–511, Dec. 2003.

[9] G. Vogel, "Avoiding flex cracks in ceramic capacitors: Analytical tool for a reliable failure analysis and guideline for positioning cercaps on PCBs," *Microelectron. Rel.*, vol. 55, no. 9, pp. 2159–2164, 2015.

[10] C. Andersson, J. Ingman, E. Varescon, and M. Kiviniemi, "Detection of cracks in multilayer ceramic capacitors by x-ray imaging," *Microelectron. Rel.*, vol. 64, no. 1, pp. 352–356, 2016. [Online]. Available: http://www.sciencedirect.com/science/article/pii/S0026271416302542

[11] L. Bechou, S. Mejdi, Y. Ousten, and Y. Danto, "Non-destructive detection and localization of defects in multilayer ceramic chip capacitors using electromechanical resonances," *Quality Rel. Eng. Int.*, vol. 12, pp. 43–53, 1996.

[12] V. Krieger, W. Wondrak, A. Dehbi, W. Bartel, Y. Ousten, and B. Levrier, "Defect detection in multilayer ceramic capacitors," *Microelectron. Rel.*, vol. 46, pp. 1926–1931, 2006.

[13] Y. C. Chan, F. Yeung, G. Jin, N. Bao, and P. S. Chung, "Nondestructive detection of defects in miniaturized multilayer ceramic capacitors using digital speckle correlation techniques," *IEEE Trans. Compon., Packag., Manuf. Technol. A*, vol. 18, no. 3, pp. 677–684, Oct. 1995. [Online]. Available: http://search.proquest.com/docview/27455226?accountid=136582

[14] D. L. Commare, "Nondestructive evaluation of MLCCs," *Ceramic Ind.*, vol. 140, no. 6, pp. 38–41, 1993.

[15] G. F. Kieran, "A comparison of screening techniques for ceramic capacitors," in *Proc. Symp. NASA Conf. Capacitor Technol., Appl. Rel.*, 1981, pp. 111–117.

[16] J. D. Prymak, "Piezoelectric effects ceramic chip capacitors (singing capacitors)," *Arrow Asian Times article*, KEMET Electronics Corporation, Aug. 2006. [Online]. Available: http://www.kemet.com/Lists/TechnicalArticles/Attachments/88/2006%2007%20ArrowAsiaTimes%20-%20MLC%20Noise.pdf

[17] J. Chen and Z. Feng, "X7r dielectric multilayer ceramic capacitors show good micro-actuating properties with little hysteresis," *Electron. Lett.*, vol. 50, no. 7, pp. 538–540, Mar. 2014.

[18] S. Levikari, T. J. Kärkkäinen, C. Andersson, J. Tamminen, and P. Silventoinen, "Acoustic phenomena in damaged ceramic capacitors," *IEEE Trans. Ind. Electron.*, vol. 65, no. 1, pp. 570–577, Jan. 2018.

[19] W. L. Johnson, S. A. Kim, G. S. White, and J. Herzberger, "Nonlinear resonant acoustic detection of cracks in multilayer ceramic capacitors," in *Proc. IEEE Int. Ultrason. Symp.*, Sep. 2014, pp. 244–247.

[20] W. L. Johnson, S. A. Kim, G. S. White, J. Herzberger, K. L. Peterson, and P. R. Heyliger, "Time-domain analysis of resonant acoustic nonlinearity arising from cracks in multilayer ceramic capacitors," in *Proc. AIP Conf. Proc.*, 2016, vol. 1706.

[21] W. I. Johnson, J. L. Herzberger, S. A. Kim, K. L. Peterson, P. R. Heyliger, and G. S. White, "Resonant acoustic frequency shifts associated with cracks in multilayer ceramic capacitors," *IEEE Trans. Device Mater. Rel.*, vol. 17, no. 2, pp. 316–323, Jun. 2017.

[22] T. J. Kärkkäinen, J. P. Talvitie, O. Ikonen, M. Kuisma, P. Silventoinen, and E. Mengotti, "Sounds from semiconductors – acoustic emission experiment with a power module," in *Proc. 16th Eur. Conf. Power Electron. Appl.*, Aug. 2014, pp. 1–6.

[23] T. J. Kärkkäinen *et al.*, "Acoustic emission in power semiconductor modules – first observations," *IEEE Trans. Power Electron.*, vol. 29, no. 11, pp. 6081–6086, Nov. 2014.

[24] T. J. Kärkkäinen, J. P. Talvitie, M. Kuisma, P. Silventoinen, and E. Mengotti, "Acoustic emission caused by the failure of a power transistor," in *Proc. IEEE Appl. Power Electron. Conf. Expo.*, Mar. 2015, pp. 2481–2484.

[25] C. Cortes and V. Vapnik, "Support-vector networks," *Mach. Learn.*, vol. 20, no. 3, pp. 273–297, Sep. 1995. [Online]. Available: https://doi.org/10.1007/BF00994018

[26] S. Levikari, T. J. Kärkkäinen, P. Silventoinen, C. Andersson, and J. Tamminen, "Acoustic detection of cracks and delamination in multilayer ceramic capacitors," in *Proc. IEEE 11th Int. Symp. Diagnostics Electr. Mach., Power Electron. Drives*, Aug. 2017, pp. 622–627.

[27] S. Levikari, "Detection of cracks: Acoustic experiments on multilayer ceramic capacitors," M.S. thesis, Lappeenranta Univ. Technol., Lappeenranta, Finland, 2018.

[28] S. Levikari, T. J. Kärkkäinen, C. Andersson, and J. Tamminen, "MLCC acoustic data set," Lappeenranta Univ. Technol., Lappeenranta, Finland, 2018. [Online]. Available:http://urn.fi/urn:nbn:fi:csc-kata20180302153714692880.

[29] S. Siuly, Y. Li, and Y. Zhang, *EEG Signal Analysis and Classification*. New York, NY, USA: Springer, 2016.

[30] M. Li, X. Liu, and X. Liu, "Infrasound signal classification based on spectral entropy and support vector machine," *Appl. Acoust.*, vol. 113, pp. 116–120, 2016. [Online]. Available: http://www.sciencedirect.com/science/article/pii/S0003682X16301761

[31] G. Dougherty, *Pattern Recognition and Classification: An Introduction*. New York, NY, USA: Springer, 2013, ch. 9.

[32] T. Fawcett, "An introduction to ROC analysis," *Pattern Recognit. Letters*, vol. 27, no. 8, pp. 861–874, 2006.

[33] JCGM, *100:2008 Evaluation of Measurement Data – Guide to the Expression of Uncertainty in Measurement*, corrected version 2010 ed. JCGM, 2010.

[34] L. Råde and B. Westergren, *Mathematics Handbook for Science and Engineering*. Lund, Sweden: Studentlitteratur, 1988, 2004.

Saku Levikari (M'18) was born in 1991 in Finland. He received the B.Sc. and M.Sc. degrees from Lappeenranta University of Technology (LUT), Lappeenranta, Finland, in May and June of 2018, respectively.

He is currently a Doctoral Student with LUT School of Energy Systems, Laboratory of Applied Electronics. His main research topics include the field of data analytics and machine learning, with main focus on wearable electronics and the reliability of power electronics.

Tommi J. Kärkkäinen (M'12) was born in 1987 in Finland. He received the B.Sc., M.Sc., and D.Sc. degrees from Lappeenranta University of Technology (LUT), Lappeenranta, Finland, in 2010, 2011, and 2015, respectively.

He is currently a Postdoctoral Researcher with LUT School of Energy Systems. His main research topic is the reliability of power electronic devices and systems, and the utilization of machine learning algorithms to improve the reliability and productivity of various systems.

Caroline Andersson (M'10) was born 1983 in Sweden. She received the M.Sc. degree from Lund University, Lund, Sweden, and the Ph.D. degree from Swiss Federal Institute of Technology, Zurich, Switzerland.

She is currently a Senior Scientist with ABB Corporate Research Center, Baden, Switzerland, on the topic of reliability of power electronics. The main focus of her research area is accelerated life testing, physics of failure, and reliability of components and systems.

Juha Tamminen was born in 1980 in Finland. He received the B.Eng. degree in electronics in 2006 from Espoo-Vantaa University of Applied Sciences, Vantaa, Finland.

He is currently a Design Manager with ABB Drives, Helsinki, Finland, in the field of production testing. His work concentrates on improving production testing concepts in pursue of better quality and productivity.

Pertti Silventoinen (M'09) was born in Simpele, Finland, in 1965. He received the D.Sc. degree from Lappeenranta University of Technology, Lappeenranta, Finland, in 2001.

He became a Professor of applied electronics in 2004. His current research interests include power electronics systems in various applications.